Effects of the Orion Launch Abort Vehicle Plumes on Aerodynamics and Controllability

Journal:	*51st Aerospace Sciences Meeting*
Manuscript ID:	Draft
luMeetingID:	1965
Date Submitted by the Author:	n/a
Contact Author:	Vicker, Darby

Effects of the Orion Launch Abort Vehicle Plumes on Aerodynamics and Controllability

Darby J. Vicker* Robert E. Childs† Stuart E. Rogers‡ Matthew S. McMullen§
Joseph A. Garcia¶ James S. Greathouse‖

The Orion Multi-Purpose Crew Vehicle (MPCV) can safely abort from a launch throughout its ascent trajectory. This paper addresses the aerodynamic controllability of the endoatmospheric abort capability, provided by a dedicated launch abort system. Computational fluid dynamics (CFD) simulations are used to characterize the aerodynamics of the launch abort vehicle (LAV). It operates between altitudes from ground level to approximately 300,000 feet, Mach numbers from 0-9, and dynamic pressure from 0-1300 psf. The aerodynamics of the powered LAV are complicated and difficult to quantify accurately by use of wind tunnel testing or CFD. Strong interactions between the vehicle flowfield and the plumes of the two solid propellant motors that provide attitude control and main propulsion contribute the main source of modeling difficulty. These interactions are a function of flight parameters such as Mach number, altitude, dynamic pressure, vehicle attitude, and parameters relating to the operation of the motors themselves – either as a function of time, or as a result of the flight control system requests for control. This paper discusses the effects of the interactions of the propulsive and attitude control motor plumes on vehicle controllability.

Nomenclature

α	Angle of Attack	C_m	Pitching Moment Coefficient
$\bar{q}$	Freestream Dynamic Pressure	C_{m_α}	Gradient of C_m to α
β	Angle of Sideslip	CFD	Computational Fluid Dynamics
Eff_{Cm}	Pitching Moment Effectiveness	CM	Crew Module
θ_{ACM}	ACM Thrust Direction	LAT	Launch Abort Tower
ACM	Attitude Control Motor	LAV	Launch Abort Vehicle
ACMTB	ACM Thrust Balance	MPCV	Multi-Purpose Crew Vehicle
ACMTR	ACM Thrust Ratio	S_{ref}	Reference Area
AM	Abort Motor	SA	Spacecraft Adapter
AMCT	Abort Motor Thrust Coefficient	SLS	Space Launch System
BPC	Boost Protection Cover	SM	Service Module
C_D	Drag Coefficient	WTT	Wind Tunnel Testing

I. Introduction

A. MPCV Components

The Orion Multi-Purpose Crew Module (MPCV) is a system being designed to carry humans to exploration destinations beyond low-earth orbit and allow them to return safely. The MPCV system, pictured in Figure 1,

*Aerospace Engineer, NASA Johnson Space Center, Professional Member AIAA
†Senior Research Scientist, STC
‡Aerospace Engineer, NASA Ames Research Center, Associate Fellow AIAA
§Senior Research Scientist, STC, Senior Member AIAA
¶Aerospace Engineer, NASA Ames Research Center, Senior Member AIAA
‖Aerospace Engineer, NASA Johnson Space Center

consists of the Crew Module (CM), the Service module (SM), the Launch Abort Tower (LAT), and the spacecraft adapter (SA). These four components are mounted at the top of the launch vehicle. During the initial design, the MPCV was intended to be launched by the Ares I rocket. Ares I used a first stage designed around a single 5-segment solid rocket booster of Space Shuttle heritage and a J-2X powered upper stage.[1] With the cancellation of the Constellation program and the Ares I launch vehicle, likely launch vehicles for the MPCV are the United Launch Alliance Delta IV Heavy for initial flight test(s) and the Space Launch System (SLS) being developed by NASA for later test flights and operational missions.[2]

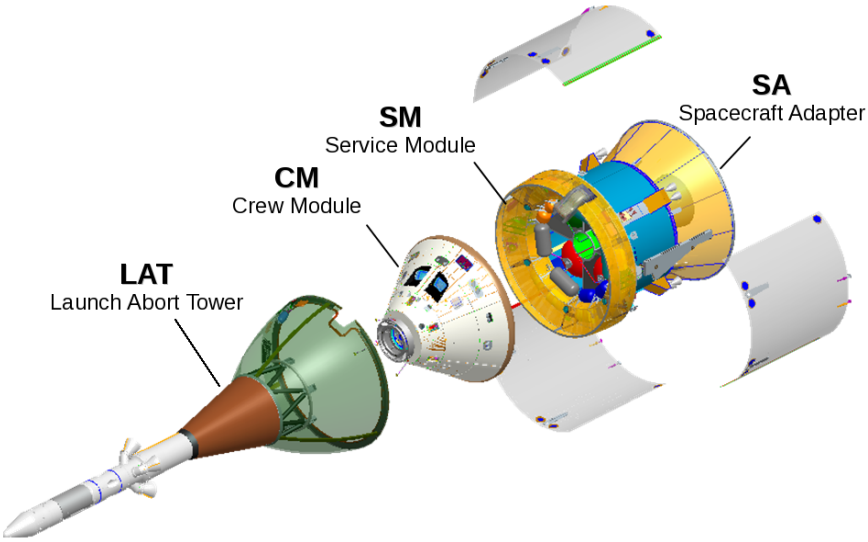

Figure 1. Major components of the MPCV

The CM provides the crew with habitable volume for all phases of flight including launch, spaceflight, and earth re-entry. As such, the CM is the central focus of the MPCV system with the other components designed largely to help the CM perform its mission. As a result, the CM contains a large number of the critical systems of the MPCV including command and control functions, life support, and landing systems. Systems placed on the other MPCV components are not needed for earth re-entry/landing and the ability to host these systems on components other than the CM allows the landed mass to be reduced. This lower landed mass has a large multiplier effect on weight and complexity of a number of other systems such as the thermal protection and recovery (parachute) systems.

The SM provides many functions for the MPCV. It provides all on-orbit attitude control and propulsion including final ascent trajectory maneuvers and pre-entry maneuvers, electrical power generation via solar panels and electrical storage, heat rejection via radiators, consumable storage (e.g. oxygen, etc.), and exo-atmospheric ascent abort capability after the LAT is jettisoned. For nominal missions the SM is separated from the CM just before atmospheric re-entry since the CM internal batteries are sized only to operate the avionics and CM systems for the period of time required for entry and recovery. During launch, the SM is covered by panels to protect it from weather while on the ground and from launch aerodynamic loads and acoustics and to provide a secondary structural load path. This secondary load path is used during the high acceleration and high aerodynamic load portion of ascent allowing a lighter central SM structure. After the high acceleration and aerodynamic loads during first stage ascent, the SM panels are jettisoned reducing mass the second stage must carry to orbit and uncovers the SM radiators to allow rejection of heat produced by the CM systems. The SM is not recovered and burns up in the atmosphere.

The Spacecraft Adapter (SA) primarily serves to allow the MPCV system to be mounted atop the launch vehicle upper stage. The SA remains attached to the launch vehicle upper stage after ascent. Different designs of the SA will accommodate various launch vehicles used to orbit the MPCV, allowing the remainder of the MPCV systems to remain largely unchanged.

The main function of the LAT is to provide the ability to pull the CM to a sufficient distance such that the CM can use its recovery system and land safely at any time before or during first stage ascent should it be necessary. The LAT also serves to cover to protect the CM from weather on the ground and from ascent loads and acoustics. During an abort, the LAT and CM remain coupled and the CM detaches from the

SM. This LAT+CM configuration is referred to as the Launch Abort Vehicle (LAV). The main propulsive force is provided by the solid propellant Abort Motor (AM) mounted immediately forward of the CM in the LAT tower. Once ignited at the start of the abort, the AM provides thrust through four nozzles canted 25° from the tower centerline and provides a fixed profile of ∼400,000 pounds of thrust for approximately three seconds with thrust tapering until burnout at approximately seven seconds. The high thrust of the AM is designed to quickly accelerate the LAV away from the pad or launch vehicle danger and propel the CM to a safe distance. The design goal is to ensure that at three seconds from the start of an abort, the LAV is a minimum of 300 feet away from the launch vehicle that continues to accelerate. The LAT must also propel the CM to sufficient altitude and distance downrange to allow safe parachute deployment and a water landing in the case of pad or low-altitude abort.

Control of the LAV is achieved by use of the Attitude Control Motor (ACM) mounted just aft of the nosecone. The ACM directs its exhaust through eight radially oriented nozzles that can independently vary their thrust. This allows the flight control system to command thrust magnitude from zero to approximately 7000 pounds and orient the resultant thrust vector radially through 360° of azimuth. Since the ACM is a solid propellant motor, it is always burning and to achieve any resultant thrust value less than maximum, opposing nozzles are opened to partially or fully cancel thrust produced by the primary nozzles. This ability to control thrust magnitude and direction allows the flight control system to achieve the desired attitude of the LAV as it flies away from the launch vehicle to a safe distance. After the initial fly-out and the LAV has slowed sufficiently, the ACM is used to re-orient the LAV from tower-forward flight to base-forward flight so that the CM heatshield faces into the freestream flow. This mimics a nominal entry attitude and allows the recovery system to be used for aborts without extensive modification after the LAT is jettisoned. Figure 2 gives an overall layout of the LAV showing the location of the ACM nozzles at the tip of the tower just below the nosecone, and the AM nozzles near the midpoint of the tower.

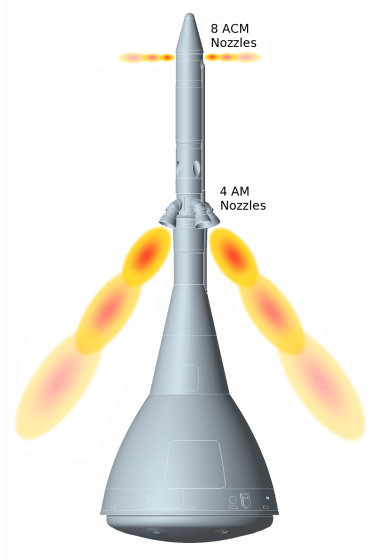

Figure 2. Location and orientation of the LAV AM and ACM nozzles

B. MPCV Ascent Abort Trajectory

For this paper we will focus on LAV aborts, which can take place from the launch pad throughout first stage flight of the launch vehicle. The LAT systems were designed with specifications that would allow aborts from the first stage of the now canceled Ares I launch vehicle. The Ares I first stage burned for approximately 150 seconds, at which time it was separated, and the second stage was ignited to propel the MPCV to a transfer orbit with the SM performing the final orbital insertion burn. During the second stage flight, thrust can be terminated reliably and aerodynamic drag force has dropped to nearly zero due to the high altitude. As a result, the lower thrust of the service module main engine is capable of performing the needed abort propulsion, and the high thrust of the LAT abort motor is unnecessary. This allows the large mass of the

LAT to be jettisoned shortly after the second stage is verified to be operating properly.

The ascent trajectory of the solid propellant Ares I launch vehicle complicated the LAV design and analysis in many ways, since the nominal ascent trajectory exceeded 900 psf with the LAV accelerating to nearly 1300 psf in some cases as a result of the AM thrust impulse. Figure 3 plots freestream dynamic pressure versus freestream Mach number for the LAV aborting from of a notional Ares I trajectory. The circular symbols represent the starting point of the abort when the AM and ACM are ignited and the LAV is separated from the SM to begin flying away from the launch vehicle. The black line indicates the LAV flight away from the launch vehicle while the AM is developing high thrust, then slowing as the drag exceeds thrust of the AM during its lower thrust and tail-off. The cyan line then continues the trajectory showing the period of time when the ACM is operating in high thrust mode after the AM has burned out, while the red line shows flight during the time the ACM is in its reduced thrust mode. The design of the ACM is tailored to provide high thrust when dynamic pressures and large disturbance torques are expected followed by reduced thrust (approximately 65% lower) to allow longer burn time where lower dynamic pressures and lower disturbance torques are expected.

Although the Delta IV-heavy and the SLS launch vehicles will not reach the level of dynamic pressure of Ares I, the overall problem of high dynamic pressure is only somewhat reduced for these launch vehicles. The large thrust and impulse of the LAT necessary to obtain 300 feet of separation in three seconds still results in high dynamic pressures during the LAV flight.

The ability for the MPCV to abort from a launch at any point before or during the ascent flight, using the LAT up to second stage ignition and the SM thereafter, greatly enhances crew safety.

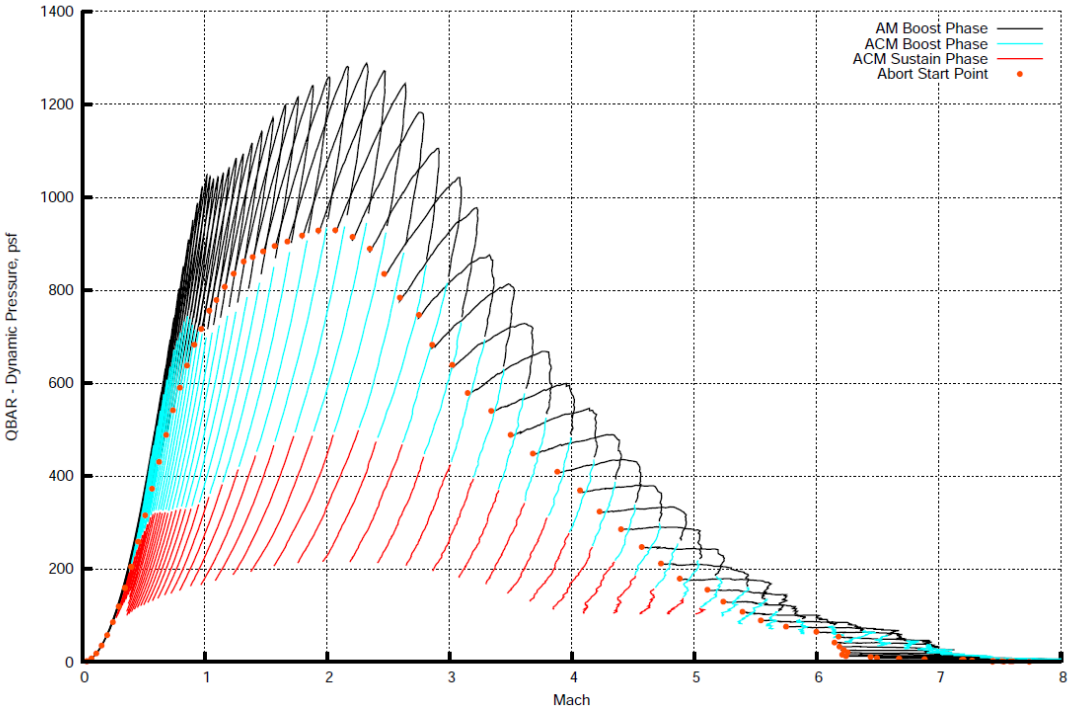

Figure 3. MPCV Abort Trajectory dynamic pressure

C. MPCV Abort Fight Control

A successful abort relies on the ability of the flight control system to maintain and control the LAV attitude at all times. This is necessary to ensure that the required trajectory is achieved and to place the crew module within the required attitude and rate envelope to ensure a successful parachute system deployment and safe landing. For LAV aborts, the flight control system's only effector is the ACM. While the details of the non-linear flight control law are beyond the scope of this paper, the vehicle pitch and yaw attitude is controlled directly by varying net thrust and thrust direction of the ACM. The LAV roll angle is controlled indirectly

by introducing a sideslip angle and utilizing the resulting aerodynamic side force acting in conjunction with the vertically offset center of mass. This provides the desired roll moment. Details of the flight control system can be found in the work by Proud et al.,[3] and McNamara et al.[4]

The gross attitude control torque available to the control system from the ACM is a function of the moment arm from the ACM nozzles to the current vehicle center of mass as well as the maximum directional thrust capability of the ACM. This maximum thrust is a function of the current motor operating conditions – primarily the chamber pressure, atmospheric pressure, and operation of "valves," referred to as pintles, in each of the eight ACM nozzles. All of these factors are mathematically modeled within the GN&C simulations.

The ACM must overcome disturbance torques from two primary sources to maintain controlled flight. One of these torques is from the offset between the AM thrust vector and the center of mass. Since in excess of 5000 lbs of propellant is consumed by the AM and ACM during the abort, and both are located on the forward part of the LAV, the vehicle center of mass moves over 20 inches aft during the abort. This requires modeling of the mass properties of the LAV as a function of time for the abort simulations. The AM nozzles are not top/bottom symmetric and are designed to produce a thrust vector that, when combined with the AM thrust profile, produces a time-integrated disturbance torque impulse that minimizes cases in which the ACM is unable to maintain the desired trajectory when combined with dispersions of all relevant parameters.

The other disturbance is from the LAV aerodynamic loads. Aerodynamic characterization of the LAV and the influence of the AM and ACM plumes interacting with the LAV surface are discussed in later sections.

D. Aerodynamic Characterization of the LAV

Characterization of the LAV aerodynamics requires an eight dimensional parametric space. This space includes dependence on the typical aerodynamic factors of Mach number, angle of attack (α), and angle of sideslip (β). Since the AM and ACM plumes interact with the flowfield around the LAV, the overall aerodynamics are also dependent on factors defining the operation of the AM and ACM, including AM and ACM gross thrust, ACM net thrust, and ACM thrust direction. To allow accurate flight simulations for all abort flight conditions, an aerodynamic database covering the entire flight envelope had to be developed. Regions in which the ACM control power was significantly degraded due to the aerodynamics and high dynamic pressures seen in some abort conditions were studied more closely.

For the MPCV program, a mix of ground based aerodynamic testing and computational methods was used to evaluate the LAV aerodynamics. Wind tunnel testing (WTT) focused on the first few seconds of the LAV flight when the AM and/or ACM motors are firing and the vehicle is at low angle of attack. Computational Fluid Dynamics (CFD) was used for high angles of attack during the LAV reorientation to place the CM in position for parachute deploy, and also for the effects of the LAV plumes at wind tunnel versus flight conditions. Modeling the LAV and plumes is a challenge for both CFD and wind tunnels. For wind tunnel testing, there are constraints due to the facility itself, cost, and model size and complexity. One key constraint for LAV testing was that only cold air could be used as the gas to simulate the hot rocket motor exhaust of the AM and ACM plumes. These constraints also prevented testing of the LAV at flight like conditions, and as such, scaling of both inertial and plume properties was required. The scaling techniques available were not able to provide a perfect match to flight conditions, limiting the accuracy of the resulting aerodynamics. CFD analysis does not have these same limitations and constraints, but deficiencies in turbulence modeling of both the high energy plumes and the base flow of the LAV limits accuracy of these simulations. This, together with the significant computational cost of each simulation precluded fully populating the database using only CFD. As a result, both CFD and ground based wind tunnel test data were employed and combined to build the final aerodynamic database. Differences between the two methods were used to partially inform the development of the uncertainty model supplied along with the database "nominal" values.

The remainder of this paper discuses the computational simulation of the aerodynamics of the LAV during abort flight. Simulations presented used the OVERFLOW[5,6] solver, which employs a structured overset-grid approach and solves the Reynolds-averaged Navier-Stokes equations. Extensive work was previously performed by the current authors to develop guidelines on the best methods to model the LAV and to produce other computational results for the LAV.[10–13]

Computing the aerodynamics of the LAV, and in particular the jet-interactions due to the AM and ACM plumes over the entire parametric space required by the aerodynamic database proved to be very challenging. In characterizing the aerodynamic performance of the LAV over this parametric space, a number of non-

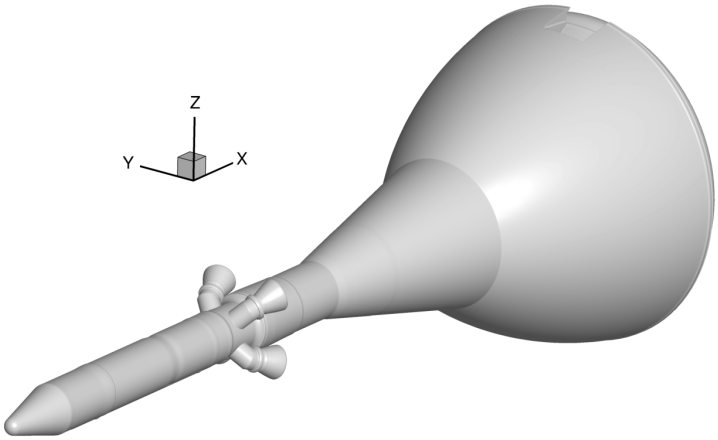

Figure 4. LAV surface

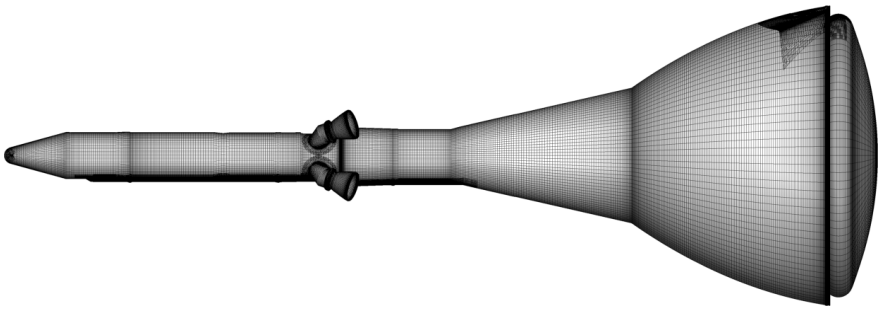

Figure 5. LAV surface grids

linear behaviors have been uncovered in both wind tunnel and computational analysis. The following section presents results and discuss the effects of the AM and AM+ACM with a particular emphasis placed on how the jet-interaction affects the control margin available to the flight control system.

II. LAV Simulations

A. Grid generation

The overset grid systems used for the analysis of the LAV are generated using an automated process programmed around the scripting system of the Chimera Grid Tools software package,[7,8] version 2.1. This script system is coded to automatically generate the surface and volume grids, generate input files for and execute pegasus5[9] for domain connectivity, then generate the input files for OVERFLOW and post-processing programs. The system also includes scripts to generate boundary condition files needed to simulate the AM and ACM jets at various thrust conditions.

Surface grids for the LAV are shown in Figures 4 and 5. In general, the stretching ratio for the surface grids is kept at 1.10 or less. A slice through the centerline of the volume grids is shown in Figure 6. The wall-normal grid spacing was selected with the goal of achieving $y^+ \leq 1$ at the first interior grid point at viscous walls, which is a useful rule of thumb for achieving good accuracy from the SST turbulence model used for calculations. A uniform wall-normal spacing was used over the entire vehicle with a stretching ratio of 1.15, and the nominal limit on y^+ was only exceeded at a small number of points on the LAV exterior, typically at convex corners. The nozzle interior walls were treated as viscous, but the target limit on y^+ was disregarded there. The dense region of Cartesian grids surrounding the body are designed to resolve

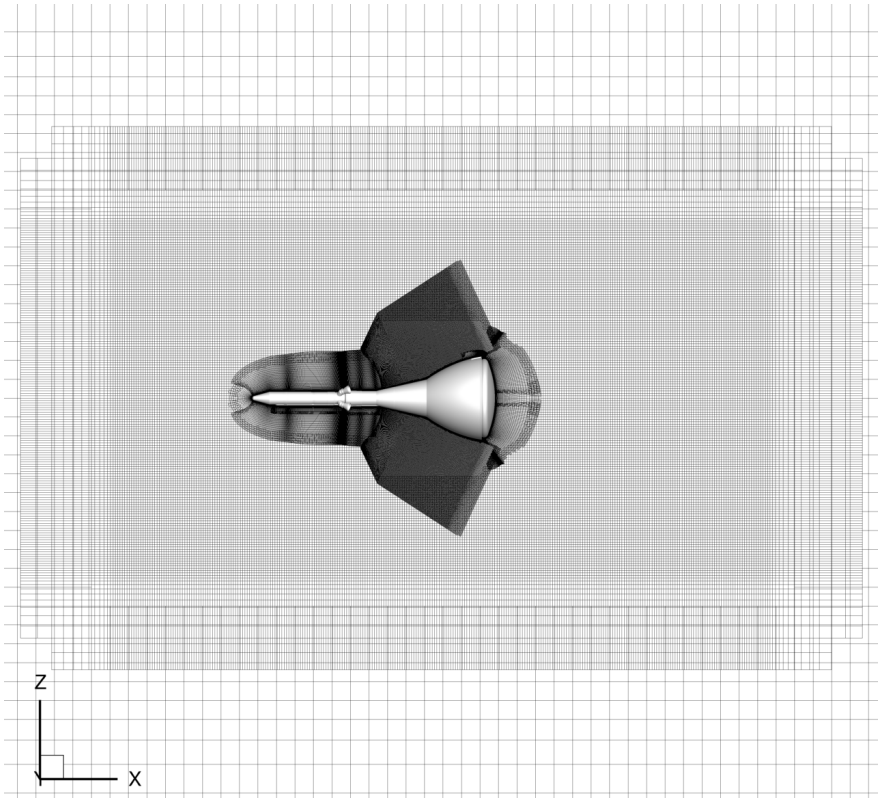

Figure 6. LAV centerline grids

the wake of the vehicle. The size of this wake "box" was chosen such that the axial extent provides good grid resolution to $\sim 1.5\times$ the length of the reversed flow wake. Additionally, the box width (and height) is sufficient to fully encompass the AM plumes and any significant effects induced in the freestream for moderate angles of attack expected during the AM burn.

The overall grid resolution was initially determined by a semi-rigorous grid resolution study. Many other improvements have been made since as a result of detailed analysis showing inadequate resolution in specific areas.[12] For example, the stream-wise resolution at the trailing edge of the vehicle was increased by almost a factor of ten to more accurately capture the expansion and match wind tunnel pressures in that region. See Figure 7 for a closeup of this detail. Another area in which the grid resolution was increased was at the exit of the AM nozzles and in the plume refinement grids. Detailed comparisons to the AM power-on wind tunnel test data showed that the CFD did not capture the correct physics due to a lack of grid resolution[12] among other things. Figure 8 shows the AM nozzle and raceway details. Note the very high stream-wise resolution near the AM nozzle exit.

The grid generation process produces grids and jet boundary conditions suitable for any combination of AM and ACM firings. The AM nozzles are always present, but if the AM jets are not firing, the jet plenum inflow boundary condition is set to be a solid wall. The only ACM nozzles included in the grid system are for those jets firing for the particular simulation. The non-flowing ACM nozzle grids are omitted from the geometry to reduce the number of grid points and lower computational cost. This simplification was made after studies indicated eliminating non-thrusting ACM nozzles had a negligible effect on vehicle aerodynamics. In order to accurately model the ACM, two grid zones are generated for each ACM nozzle: a cylindrical nozzle-fitted grid which wraps from the inside of the nozzle up to the outer surface of the LAV, and an overlapping grid inside the core of the nozzle. The surface and volume grids on the LAT tower in the vicinity of the ACMs are also refined when the ACM nozzles are present to better resolve the high gradients created by the plumes. A close-up of the surface grids in the vicinity of the ACMs and a cross-section of one of the ACM nozzles is shown in Figure 9.

The gridding of the AM nozzles is topologically similar to that of the ACM nozzles; it includes a body-

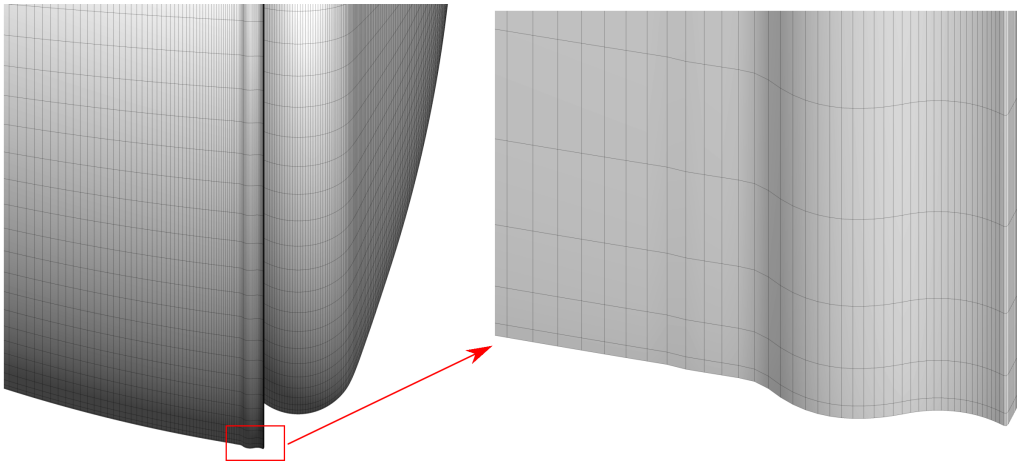

Figure 7. LAV aft lip

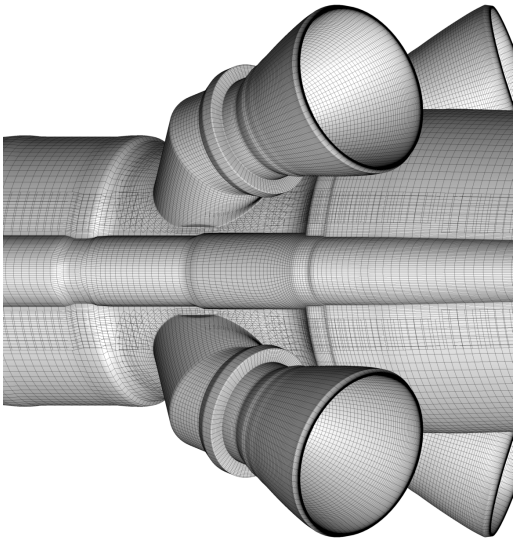

Figure 8. LAV AM and raceway

fitted and overlapping core grid. In addition, there are several plume refinement grids. For each AM nozzle, there is a near-nozzle plume refinement grid that extends 4 nozzle diameters in the axial direction. The radial spacing near the AM lip is very fine and is intended to resolve the AM plume shear layer. The spacing in the radial direction becomes uniform at the downstream end of the near-nozzle plume refinement grid. The axial spacing near the AM lip is the same as the radial spacing, resulting in nearly uniform cells at the nozzle lip, and increases to a larger value at the downstream boundary. A two-dimensional version of this grid is built and revolved about the nozzle symmetry axis with uniform spacing in the circumferential direction. The axis is removed and replaced with an overlapping core grid, similar to what is done with the nozzle-fitted grid. The flow gradients from the four near-nozzle plume refinement grids are carried downstream by a single far-nozzle plume refinement grid. This grid is very similar in topology to the near-nozzle grids but instead is revolved about the vehicle's X-axis. See Figure 10 for an illustration of the nozzle geometry and the plume refinement grids. The grid systems typically contain on the order of 60 zones and approximately 90 million grid points. There are approximately 33 million grid points in the abort motor plume refinement grids alone.

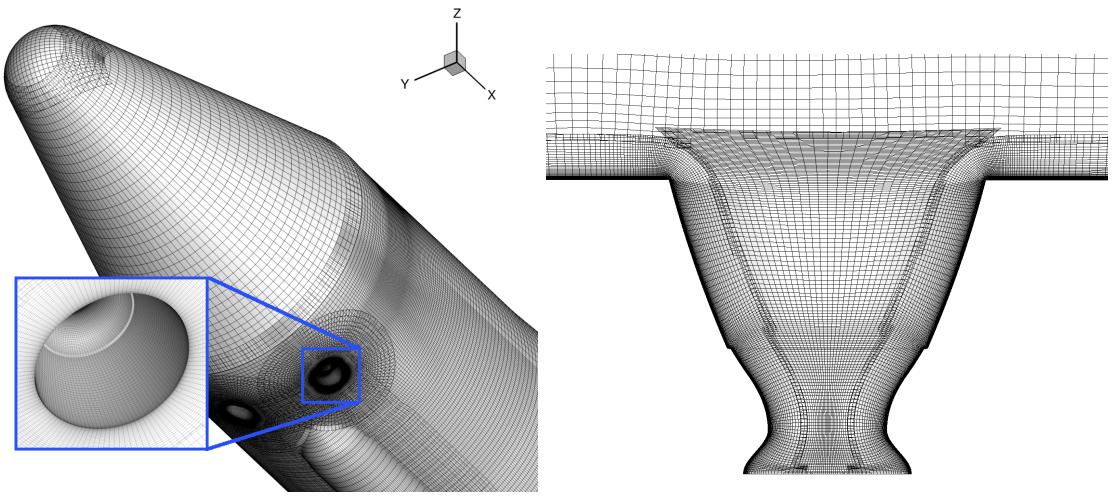

Figure 9. Attitude control motor nozzle geometry and grids

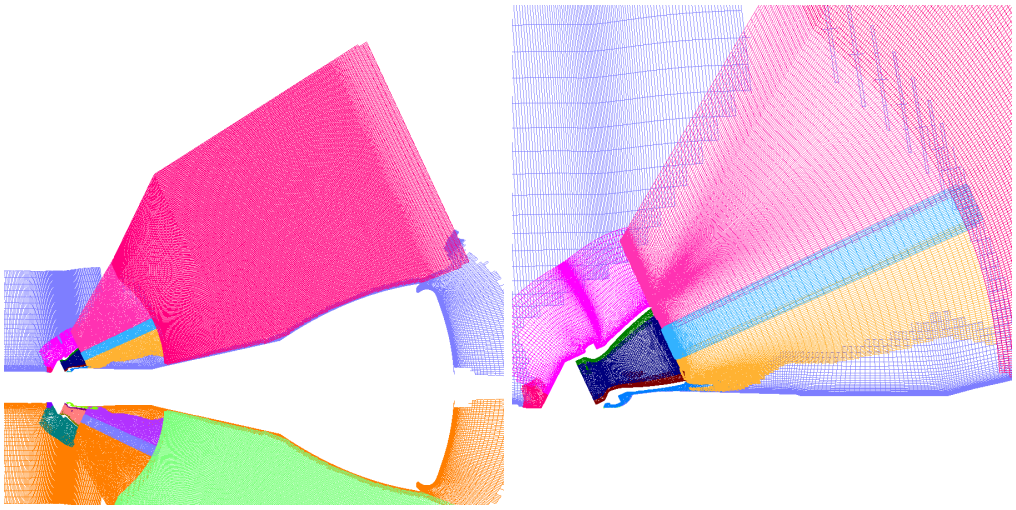

Figure 10. Abort motor nozzle geometry and plume refinement grids

B. Computed results

1. AM Interactions

The AM effects on pitching moment is a strong function of the vehicle Mach number and the AM thrust coefficient (AMCT). AMCT is defined as the AM thrust normalized by the freestream dynamic pressure ($\bar{q}$) and vehicle reference area (S_{ref}) resulting in a non-dimensional thrust coefficient similar to that of Drag Coefficient (C_D).

$$AMCT = \frac{Thrust}{\bar{q} * S_{ref}}$$

In order to gain some insight into the aerodynamics of the LAV while the AM is firing, it is useful to consider a fixed angle of attack and sideslip, and vary the Mach number at a fixed AMCT value. One figure of merit for vehicle control is the static stability, or the tendency of the vehicle to return to the trim state if disturbed. One measure of static stability often used is the pitching moment derivative with respect to alpha (C_{m_α}). Figure 11 illustrates C_{m_α} versus Mach number at AMCT values of 0 (AM not firing), 2, 3, and 4 represented by four separate curves. Typically, a negative value of C_{m_α} is desired as this will result in increasing restoring moment as the vehicle attitude moves away from the trim condition. However, this

correlation of C_{m_α} and stability will only hold if the vehicle has locally linear aerodynamics and only for C_{m_α} computed around the trim point. It is common for vehicles to have areas of positive C_{m_α} away from a trim condition but remain stable due to an overall restoring torque despite a locally positive slope.

Figure 11 shows that without the AM affecting the LAV aerodynamics (black "power off" line) the LAV has a desirable negative C_{m_α} for all Mach numbers. With the AM firing however, the plumes from the four aft facing nozzles interact with the freestream flow and change the aerodynamics to produce Mach ranges with unstable pitch slope and non-linearities of the aerodynamics versus Mach number. The Mach number region in which instability occurs, and the magnitude of the instability is a strong function of AMCT. At an AMCT ratio of 2 (blue line), the pitching moment slope is unstable from Mach 1.05 to 2 and at again at Mach 6. For all Mach numbers at this AMCT, the AM jet-interaction is either detrimental to vehicle stability or has near zero effect. Stability is most affected in the high transonic range where dynamic pressures are also largest, creating a higher likelihood of control difficulty.

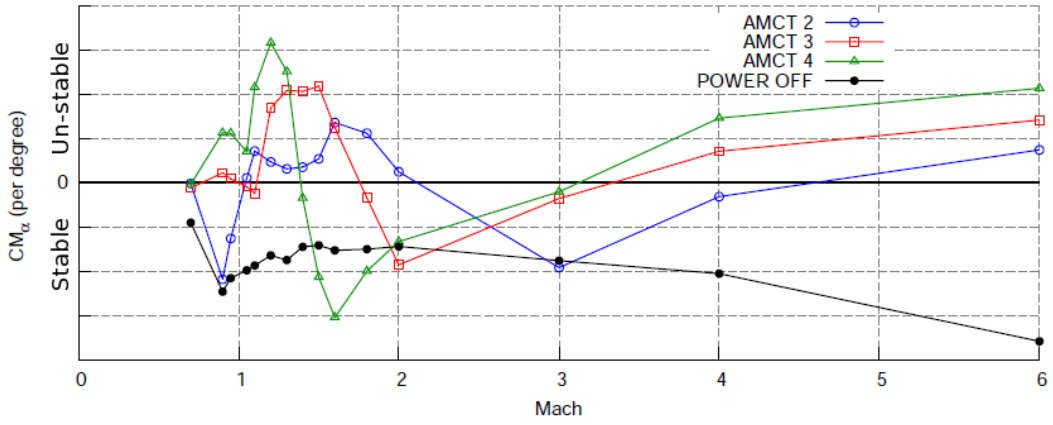

Figure 11. LAV Pitch Stability with and without AM firing

Comparing the aerodynamics at an AMCT ratio of 3.0 to the AMCT ratio of 2.0, the instability produced by the AM jet-interaction peaks at a larger magnitude, but occurs in a narrower range of Mach number – from 1.1 to 1.8 – as shown in Figure 11 by the red line. At this power condition, the AM effect is destabilizing at all Mach numbers with the exception of Mach 2.0, although the overall vehicle retains a stable C_{m_α} from approximately Mach 1.8 to 3.3.

At a thrust coefficient of 4.0 (green line in Figure 11) the destabilizing effect of the AM plumes again grows larger in magnitude, but is further compressed in Mach number to below 1.4. All three AMCT values show a similar pattern of increasing instability up to a maximum in the transonic Mach range, followed by a reduction of the effect to very small or even slightly stabilizing values, followed by another increase to unstable values at high Mach. The Mach number at which these maxima and minima occur are compressed toward the low Mach range with increasing AMCT. As a result, the higher AMCT conditions exhibit a much more non-linear aerodynamic response to Mach number.

It is also useful to consider the variation of the AM jet-interaction as a function of AM thrust coefficient at a fixed Mach number. This reveals a strong dependence of the aerodynamics to the plume thrust coefficient. This behavior is in large part driven by the shape of the AM plumes changing as a function of AMCT. The AM plumes are, at most flight conditions, comprised of several shock cells that are formed as the under-expanded AM combustion gasses initially flow out of the nozzle and turn outward into the lower ambient pressure conditions and then turn back inward necessitating a strong shock. This defines the first shock cell, and as the plumes central pressure is increased by this strong shock, the plume again expands and repeats the cycle. The length and size of these shock cells is dependent on the AM chamber pressure and the freestream conditions into which the plume is flowing. As the AM plumes are largest in diameter at a point approximately halfway between the strong shocks, and narrowest at these shocks, movement of these features changes the distance between the LAV surface and the very high velocity/ high energy shear layer of the plume. Interaction between these plumes and the surface can result in drastic changes in surface pressure and thus drive large variations in the vehicle stability. Figure 12 shows the plume shape as AMCT is increased from 2.0 to 6.0 at a flight condition of Mach 0.7 and 10° angle of attack. Here the flowfield is

contoured by Mach number with the blue range representing low values and the red range representing high values, and the surface is contoured by surface pressure coefficient. The effect of the plume as it passes near the surface can be seen as it creates a region of low pressure. The much higher velocity of the plume core entrains flow between it and the surface, acting as an ejector and resulting in a localized low pressure area. In conditions where the plume core impinges directly on the LAV surface, the high energy in the plume creates a region of high pressure. For the conditions shown in Figure 12, the plume core passes sufficiently close to the surface to create a large region of low pressure. This low pressure region closely tracks the maximum diameter of the third shock cell as AMCT is increased. The third shock cell moves aft of the LAV surface between AMCT=5 and AMCT=6, with a new low pressure area forming under the second shock cell maximum diameter.

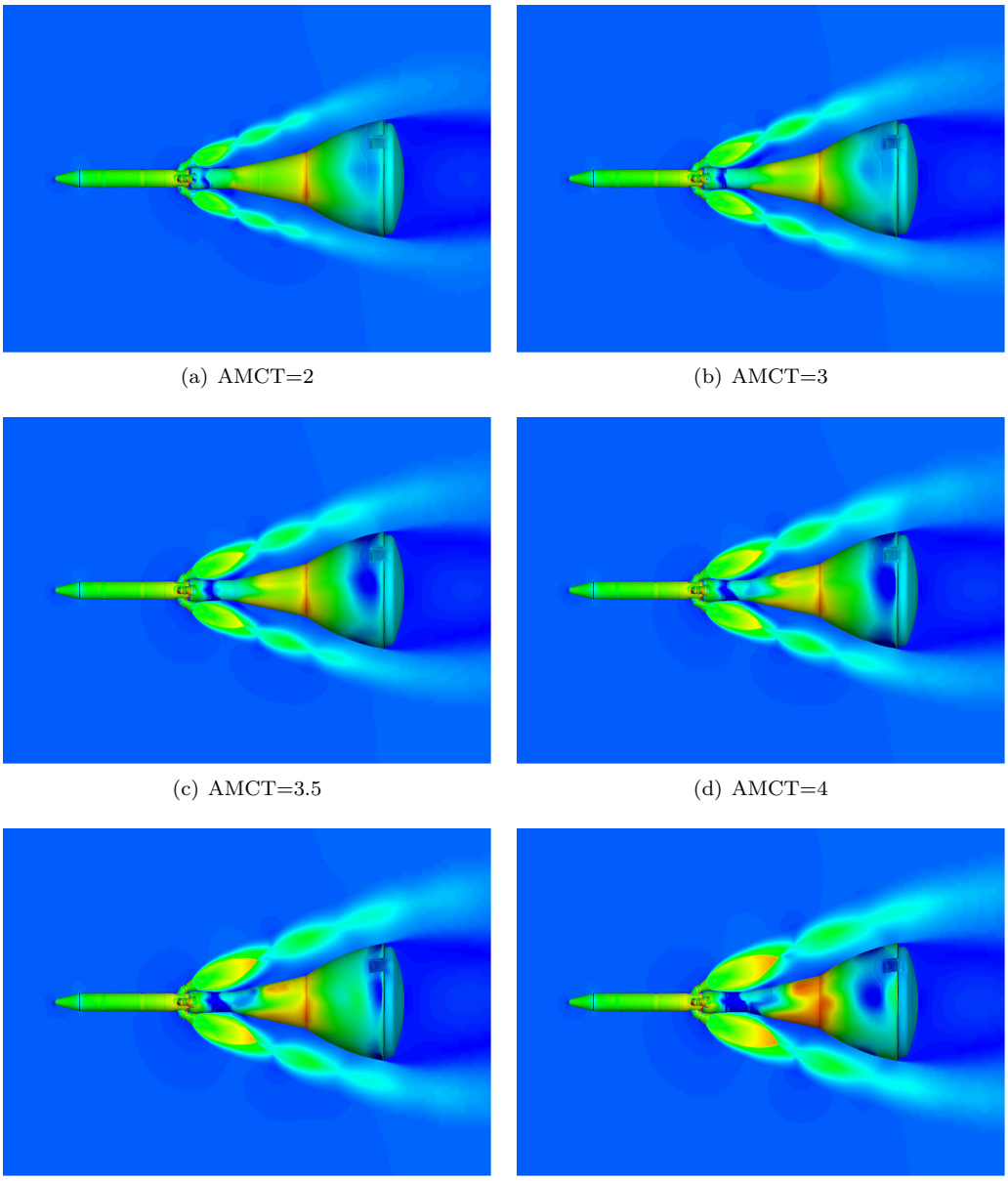

(a) AMCT=2 (b) AMCT=3

(c) AMCT=3.5 (d) AMCT=4

(e) AMCT=5 (f) AMCT=6

Figure 12. AM Plume Flow Visualization for Mach = 0.70, $\alpha = 10^{\circ}$

The integrated effect of these large pressure changes mostly cancel as the opposing plume behavior is similar, but small asymmetries between plume pairs can have large impacts on the vehicle stability due to the large magnitude of pressure change and the large area affected. The two plots in Figure 13 show the

integrated effect of the surface pressure changes due to the AM plumes interacting with the LAV. These plot $\Delta C_{m,CG}$ versus CT at 10° angle of attack for both Mach 0.9 and Mach 1.1, where $\Delta C_{m,CG}$ is the difference in pitching moment about the center of gravity between the power-on and power-off conditions. For all thrust coefficient values, the jet-interaction increment is positive and thus destabilizing. In addition, the behavior is very non-linear – the selected points for analysis are separated by at most 0.25 AMCT and yet are not fully sufficient to define the shape of the curve. This is especially true for the Mach 1.1 condition from AMCT=0.75 to 2.5 where the pitching moment increment cycles through 5 reversals of slope.

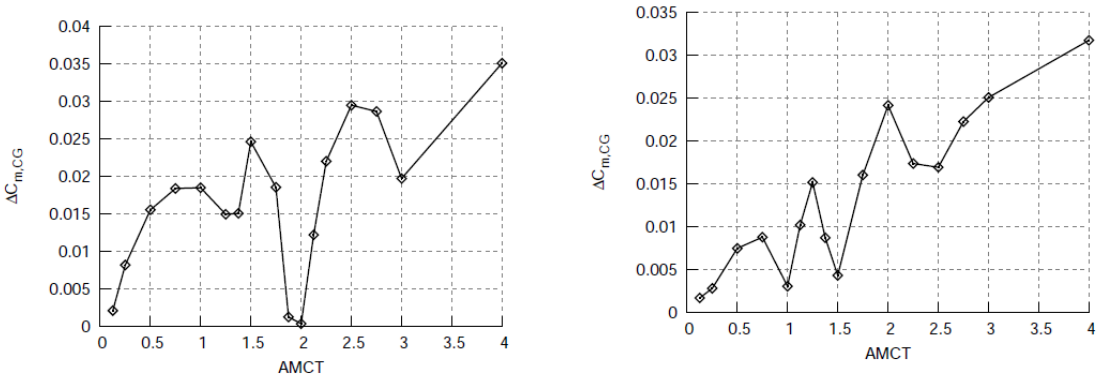

(a) Mach 0.9 (b) Mach 1.1

Figure 13. AM Plume interaction versus AMCT at $\alpha = 10°$

Unfortunately, asymmetry between the pairs of plumes are unavoidable and are in effect built into the LAV, as the CM center of mass is offset in order to produce a trim angle of attack during atmospheric entry. This offset CM center of mass also results in the LAV center of mass being offset from the centerline and requires that the AM thrust vector be canted to reduce undesirable torque produced during the AM burn. This thrust vector canting is done by of use of slightly smaller nozzles throats in the AM nozzles opposite of the LAV mass center. This slightly reduces the thrust relative to the opposing two nozzles and cants the resultant total thrust vector so that its line of action passes close to the center of mass and minimizes the disturbance torque. As a result, the opposing AM plumes have slightly different pressure ratios, and thus the shock cell structure and plume diameters are not symmetric. Other factors also influence the plume asymmetry and thus the aerodynamic interaction. At angle of attack, the AM plumes on the windward side will be more directly exposed to the freestream flow and will be pressed toward the center of the vehicle more than their counterparts on the leeward side. In addition, for supersonic flows, the shockwave that forms in front of the AM plumes will be stronger on the windward side of the vehicle, creating a higher pressure into which the AM plumes expand. This will change the pressure ratio and thus the shock cell formation and shape of the AM plumes.

At positive angle of attack, positive values of $\Delta C_{m,CG}$ are undesirable as they indicate a reduction of the vehicle stability and are likely to require more ACM thrust to maintain attitude. For this condition shown in Figure 13, the maximum positive moment coefficient generally increases as AMCT is increased, but the behavior is highly non-linear. As the LAV accelerates during an abort through the transonic range, Mach number will be increasing and AMCT will decrease. These curves indicate a significant difficulty in accurately predicting the amount of AM jet-interaction induced C_m that the vehicle will encounter. However this analysis does indicate that the interaction will be no more than $\Delta C_{m,CG}$=0.35 for these conditions. At a AMCT=2.5 and assuming full AM thrust, the ACM has a total C_m authority of approximately 0.09. Negating the AM interaction thus requires about one third of the theoretical thrust capability of the ACM. This results in only two thirds of the ACM gross torque being available to overcome disturbance torques and to actively control the LAV for trajectory shaping.

Approximately 2600 CFD simulations of the LAV with AM firing were generated to help with production of the aerodynamic database. These solutions were used to provide a WTT to flight correction, fill gaps in the WTT dataset, and to extend the range of Mach, Alpha, and AMCT beyond that collected experimentally. While AM only interactions are informative and useful in database generation, the LAV never operates with

only the AM firing. At all times during an abort when the AM is operating, the ACM is also operating in its high thrust mode. As the ACM is also a solid propellant motor it is always expelling combustion gasses, and the forward location of the ACM nozzles results in the ACM plumes continuously interacting with the freestream changing the local environment of the AM plumes. It is the combined effect of the ACM+AM interactions on the LAV aerodynamics that is the critical parameter relating to the LAV controllability. The following section will discuss the computational modeling of both the AM and ACM plumes in combination.

2. ACM and AM Interactions

This section highlights some of the computed results in which both the ACM and AM jets are firing. The goal of these simulations is to provide ACM jet-interaction increments in the forces and moments. These increments are measured as the difference between firing both the ACM and AM jets versus firing just the AM jets.

The eight ACM nozzles are arranged 45° apart circumferentially in an axial location just aft of the LAT nose, and are spaced 22.5° on either side of the pitch and yaw planes of the vehicle. The ACM system parameters include the resultant-thrust direction (θ_{ACM}), the thrust balance (ACMTB), and the ACM thrust ratio (ACMTR). The thrust direction describes the circumferential angle of the resultant thrust vector relative to the +Z pitch plane. The thrust balance is the ratio of the resultant-thrust magnitude to the total ACM system thrust with values ranging from 0.5 for zero net thrust to 1.0 for maximum directed thrust. Note that at ACMTB=0.5, θ_{ACM} is undefined. In practice, θ_{ACM} is the value just before ACMTB=0.5 was reached. The ACMTR is the total system thrust divided by the product of the freestream dynamic pressure and the vehicle's reference area, similar to the AMCT defined previously. Figure 14 illustrates the sign convention for θ_{ACM} as well as two representative ACMTB configurations.

$$ACMTB = \frac{Resultant\ Thrust}{Total\ System\ Thrust}$$

$$ACMTR = \frac{Resultant\ Total\ System\ Thurst}{\bar{q} * S_{ref}}$$

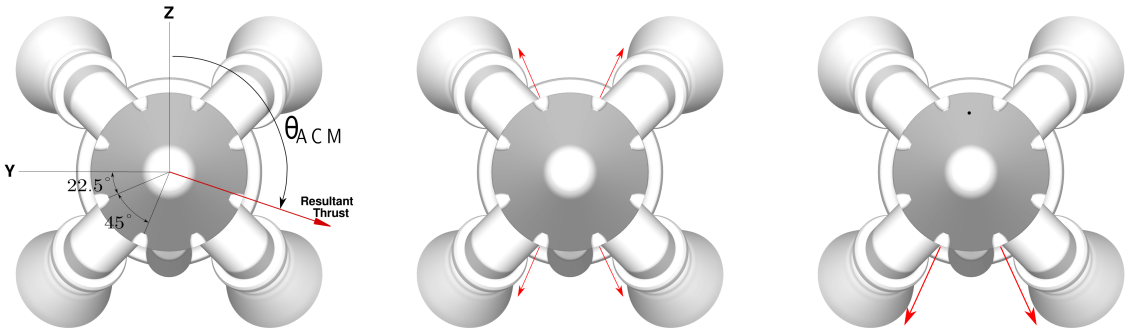

(a) θ_{ACM} sign convention (b) ACMTB=0.5 (c) ACMTB=1.0

Figure 14. ACM notations and sign conventions

Thrust from each of the eight ACM nozzles can be controlled independently using pintle valves, under the constraint that the ACM solid-motor exhaust must be vented through at least two or more of the nozzles in order to prevent internal pressure in the combustion chamber from rising above design limits. The three ACM parameters can be commanded to many thousands of configurations and as a result, only a small fraction of the configuration space has been studied using CFD simulations to date, although analysis is ongoing. Even so, over 540 CFD simulations were run with ACM jets firing for the most recent LAV design, with many others run previously on now obsolete configurations. Only one combination of these parameters is presented here: the ACM thrust-direction is along the +Z body axis ($\theta_{ACM} = 0°$), ACMTB is set to 1.0, and ACMTR is 0.04. This configuration uses equal thrust through the two nozzles on either size of the pitch plane on the -Z side of the LAT.

A good way to quantify the interaction aerodynamics of the ACM and AM plumes is in terms of the "pitching moment effectiveness". The ACM pitching moment effectiveness Eff_{Cm} is defined as:

$$Eff_{Cm} = 1 - \frac{CMJI}{CMJT}$$
$$CMJT = Cm_{total\_no\_thrust} - Cm_{total}$$
$$CMJI = Cm_{total\_no\_thrust} - Cm_{ACMoff}$$

where $Cm_{total\_no\_thrust}$ is the pitching moment excluding the ACM thrust components, Cm_{total} is the pitching moment with the ACM thrust components included, and Cm_{ACMoff} is the pitching moment for the corresponding ACM power-off case. Values of Eff_{Cm} near 1.0 indicate that the net jet interference is small relative to the moment provided by the ACM jets. Values well below 1.0 indicate a significant jet interference, and if the effectiveness goes to zero the ACM jet interference exactly offsets the moment produced by the jets. Negative effectiveness indicates a control reversal while values above 1.0 represent areas where control power of the ACM is amplified beyond the requested value. Figures 15 and 16 shows the computed ACM pitching moment effectiveness plots versus α for the different freestream Mach conditions. Each AMCT value is plotted as a separate curve. The lowest effectiveness tend to occur at Mach=0.90, AMCT=4, Mach=1.1, AMCT=3, and at Mach=1.6, AMCT=4.

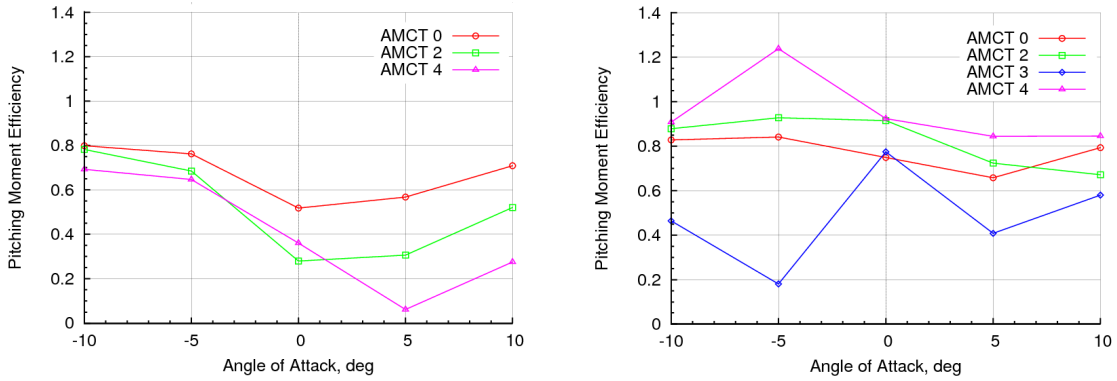

(a) Mach=0.9 (b) Mach=1.1

Figure 15. Transonic ACM effectiveness versus angle of attack

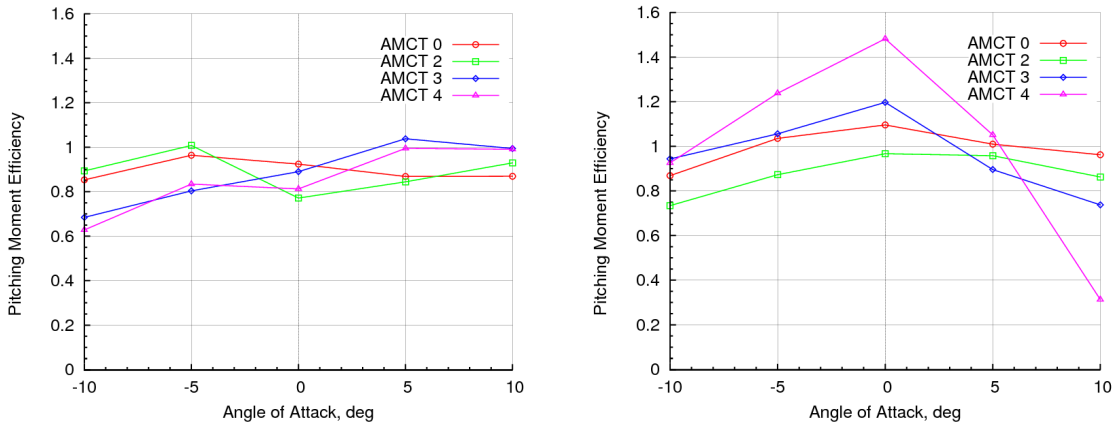

(a) Mach=1.3 (b) Mach=1.6

Figure 16. Supersonic ACM effectiveness versus angle of attack

Figures 17 to 26 illustrate the flowfield around the vehicle with the AM firing, both with and without the

ACM jets firing. These figures color the surface of the vehicle with pressure coefficient contours, and include contours of local Mach number in a cutting plane immediately aft of the vehicle. Shock waves around the LAV are revealed by gray-scale contours of the density gradient magnitude on a plane at constant Y that passes through the centers of the exit planes of the starboard nozzles. Also included are semi-transparent iso-surfaces of Mach number used to illustrate the plumes from the AM and ACM nozzles.

At Mach=0.9 and α=5°, the ACM effectiveness is very low. In this case the ACM jet-interaction reduces the desired torque from the ACM in excess of 90 percent – leaving a very small control torque to fight other disturbances such as the AM motor thrust alignment or disturbance torques due to proximity interference from the launch vehicle. The flowfield plots in Figure 17 illustrate both the ACM-on and ACM-off solutions for AMCT=2, Mach=0.9, α=5°. These show that the ACM plumes change the interaction of the bottom two AM plumes with the LAV ogive, referred to as the boost protective cover or BPC. It appears that the ACM plumes block the on-coming freestream flow such that the AM plumes remain further away from the LAV BPC than in the ACM-off solution. The slight difference in the location of the AM plumes is evident in the Mach contours directly aft of the heatshield, and in the plume iso-surfaces. When the AM plumes brush closer to the BPC lower surface, the pressure contours show lower pressure on the bottom of the BPC, and higher pressure when the AM plumes are further from the BPC. The higher pressure on this region of the BPC in the ACM-on solution causes more of a nose-down, or lower, pitching moment compared to the ACM-off solution. This nose-down pitching moment acts counter to the nose-up pitching moment imparted by the force of the ACM jets, thus the pitching moment effectiveness is low for this case. In terms of vehicle control, it is fortunate that this case is unlikely to result in the LAV departing from controlled flight, as the ACM thrust is producing additional pitch-up moment when the vehicle is already at 5° angle of attack. If the vehicle were in danger of departing, the ACM would request a firing pattern using the +Z jets and result in a jet-interaction more similar to the -5° angle of attack value, where the ACM jet-interaction is not as attenuated. Figure 18 shows solution plots at the same conditions except with AMCT=4. This higher AM thrust is evident in the larger AM plumes. These two images show a similar ACM jet-interaction occurring, and because of the larger AM plumes, it appears to affect a larger area on the BPC. As a result, the ACM effectiveness is even lower in this case.

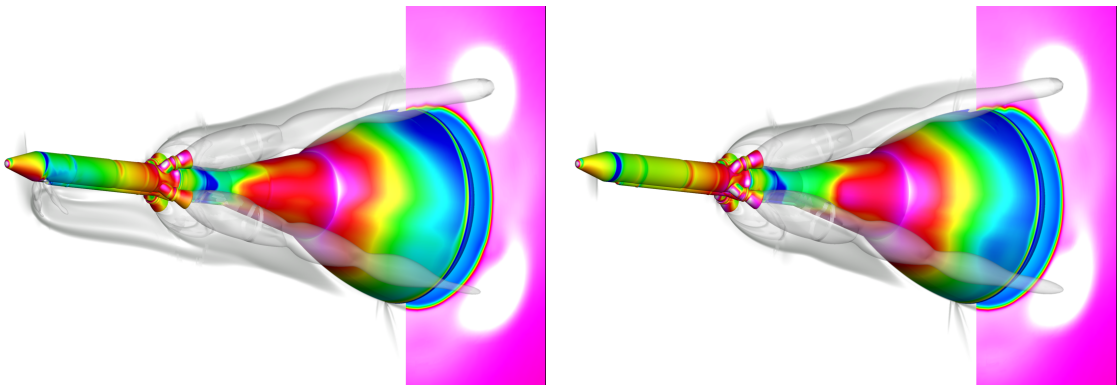

Figure 17. Flowfield of ACM-on (left) and ACM-off (right) solutions for AMCT=2, Mach=0.9, and α=5°

In Figures 20 through 24 several solutions at Mach=1.1 are shown. These transonic cases all show a normal shock near the nose of the vehicle, and a normal shock at the front end of the BPC where the cross-sectional area of the vehicle is rapidly increasing. The BPC shock causes the AM plume to undergo a sharp reduction in size. Figure 19 is a plot with Mach contours in a 45° cutting plane through the center of the AM nozzles and a stream-wise constant plane just aft of the heatshield. Also shown are gray-scaled surface pressure coefficient contours where the lowest surface pressure is colored with dark blue. This is from the Mach=1.1, α=5, AMCT=4 solution. This figure illustrates the effect of the BPC shock on the AM plumes. Aft of this the AM plumes expand again causing them to pass in close proximity to the aft portion of the BPC, resulting in regions of low surface pressure. Small changes in angle of attack, AMCT, and ACM interactions can result in large changes in the vehicle forces and moments depending on the AM plume interaction with the BPC.

In Figures 20 and 21 the solutions for Mach=1.1 and α=-5° are plotted for AM thrust values of AMCT=3 and AMCT=4, respectively. The AMCT=3 case has very low pitching moment effectiveness, while the

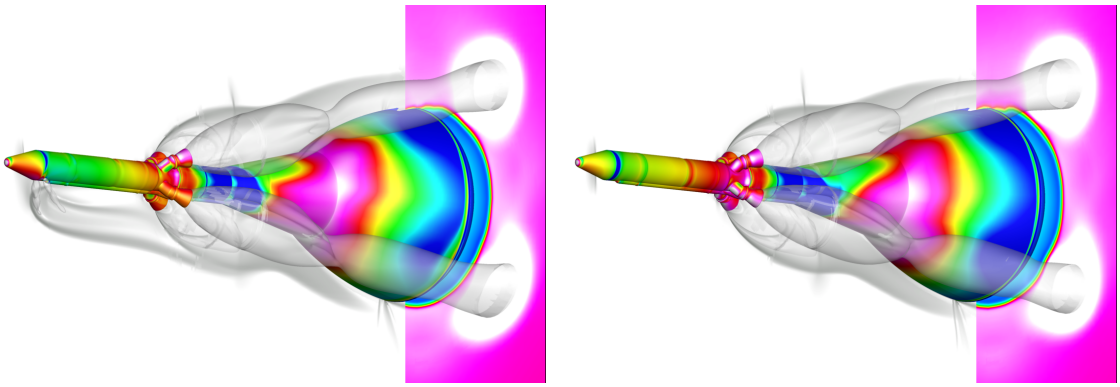

Figure 18. Flowfield of ACM-on (left) and ACM-off (right) solutions for AMCT=4, Mach=0.9, and α=5°

AMCT=4 case has a value greater than 1.0. The figures show that the AMCT=3 ACM-off case has low pressures on the bottom-aft end of the BPC caused by the AM plumes, but turning on the ACMs eliminate this low pressure, resulting in a strong nose-down pitching moment and low ACM effectiveness. However, with the larger AM plumes in the AMCT=4 solution, this effect is reversed, and the ACM effectiveness is greater than 1.0. In Figures 22, 23, and 24, the solutions for Mach=1.1 and α=5° are shown for values of AMCT=2, AMCT=3, and AMCT=4, respectively. Similar effects are seen in the ACM interactions, where the increasing AM thrust levels reverse the effect of the ACM interactions.

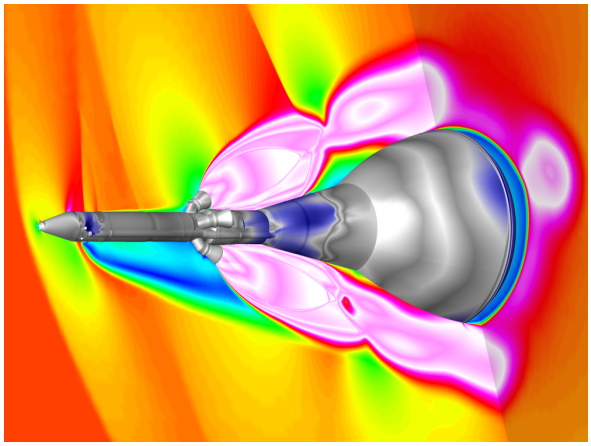

Figure 19. Off-body Mach contours and surface pressure-coefficient contours for ACM-on solution at AMCT=4, Mach=1.1, and α=5°

The solutions at Mach=1.6 and AMCT=4 are shown in Figures 25 and 26, for α=0° and α=10°, respectively. Recall that Figure 16 showed that the α=0° case had an effectiveness greater than 1.0, while the α=10° case was significantly less than 1.0. At α=0° several effects of the ACM plumes are evident at this supersonic speed. The ACM plumes changes the location of the shock caused by the AM nozzles and plumes, and this causes higher pressure on the lower AM nozzles and lower pressure on the upper AM nozzles. This increases the nose-up pitching moment. The interaction of the AM plumes with the BPC is also altered, such that the lower AM plumes generate lower pressure on the BPC, also increasing the pitching moment. Thus at these conditions, the ACM jet interaction enhances the pitching moment. The α=10° solutions also show a change in the shock locations when the ACMs are firing. At this angle of attack, however, the opposite effect is seen on the pressure on the AM nozzles. There is also a larger area of low pressure on the tower just aft of the ACM nozzles, causing a nose-down pitching moment. Finally, the impingement of the AM plumes on the BPC causes higher pressures when the ACMs are firing, which also creates a nose-down pitching moment. These all contribute to the low ACM effectiveness at this condition.

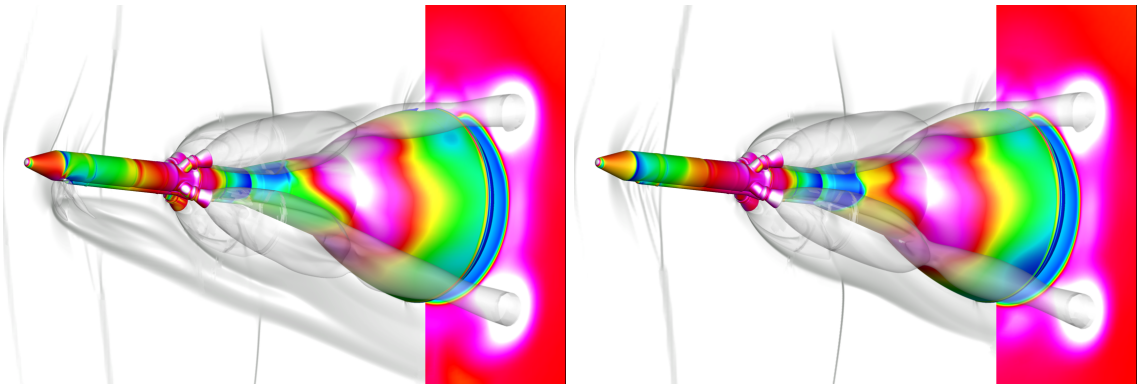

Figure 20. Flowfield of ACM-on (left) and ACM-off (right) solutions for AMCT=3, Mach=1.1, and α=-5°

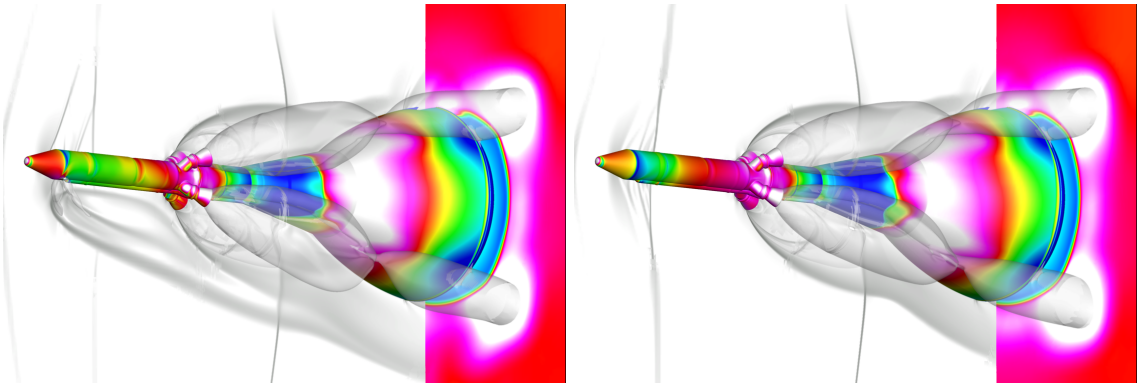

Figure 21. Flowfield of ACM-on (left) and ACM-off (right) solutions for AMCT=4, Mach=1.1, and α=-5°

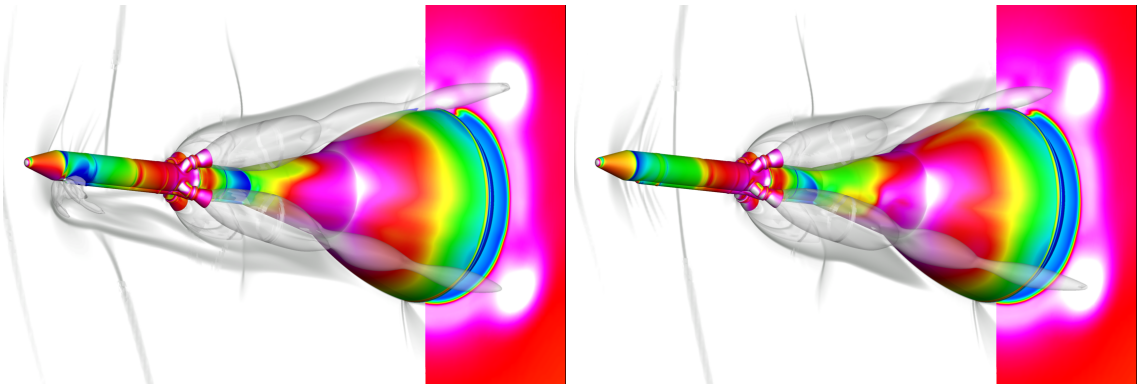

Figure 22. Flowfield of ACM-on (left) and ACM-off (right) solutions for AMCT=2, Mach=1.1, and α=5°

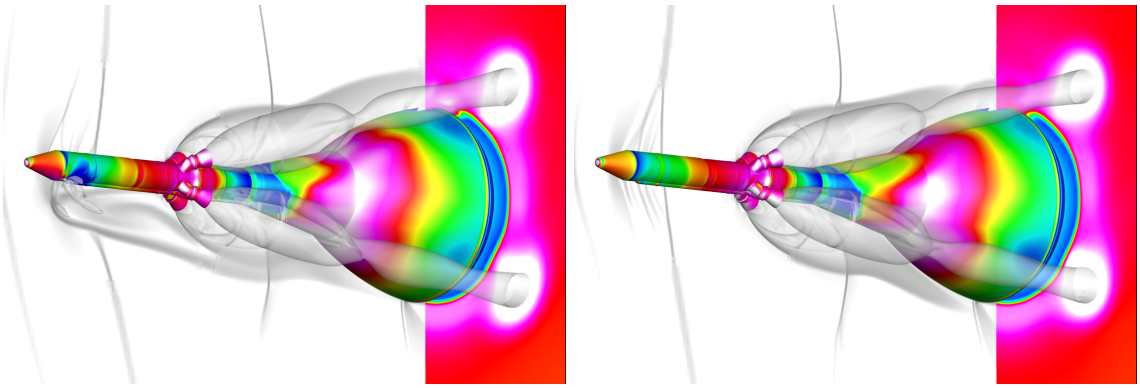

Figure 23. Flowfield of ACM-on (left) and ACM-off (right) solutions for AMCT=3, Mach=1.1, and α=5°

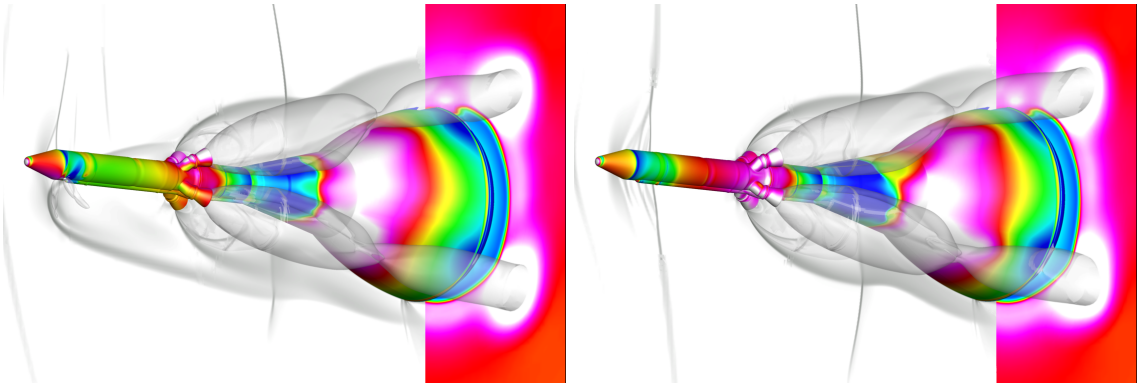

Figure 24. Flowfield of ACM-on (left) and ACM-off (right) solutions for AMCT=4, Mach=1.1, and α=5°

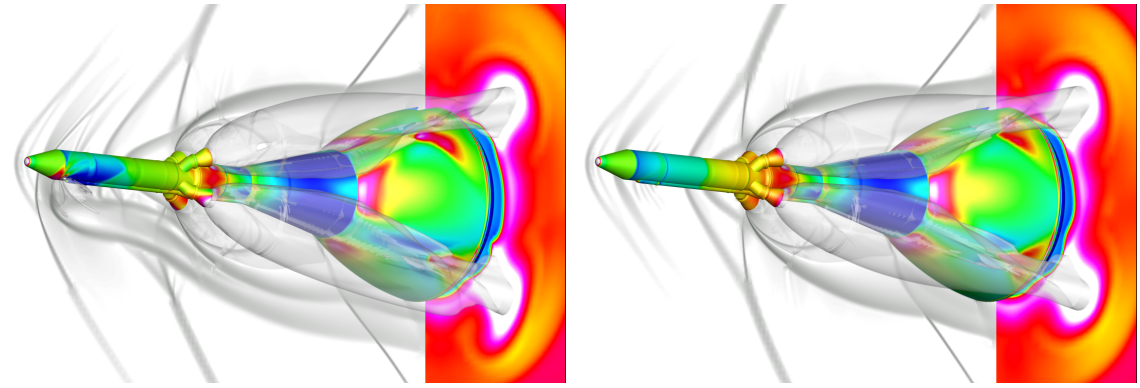

Figure 25. Flowfield of ACM-on (left) and ACM-off (right) solutions for AMCT=4, Mach=1.6, and α=0°

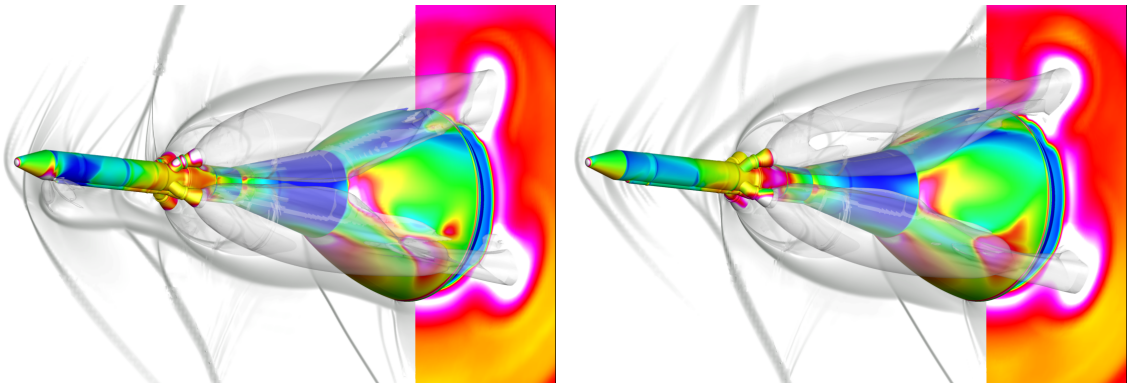

Figure 26. Flowfield of ACM-on (left) and ACM-off (right) solutions for AMCT=4, Mach=1.6, and α=10°

III. Conclusion

The aerodynamics of the Orion launch abort vehicle (LAV) were simulated using the CFD solver OVERFLOW. The goal of this work was to provide aerodynamic data to support the development of a comprehensive aerodynamic database, which was then used in the design of the vehicle control system and to assess vehicle controllability. Both wind tunnel and CFD data were used for database development, and each technique has strengths and weakness in its ability to replicate true flight aerodynamics. The vehicle's aerodynamics are complicated due to interactions of the control and propulsive jet plumes with themselves and the freestream flow around the LAV. The CFD results provide the ability to visualize and understand many of the jet-interactions which affect LAV controllability. The aggregate data of wind tunnel testing and several thousand CFD simulations of the LAV was used to produce the MPCV LAV aerodynamic database and allow flight simulation of aborts covering the entire LAV abort flight envelope.

References

[1]Stanley, D. O., Cook, S. A., Connolly, J., and Hanley, J. M., "Exploration Systems Architecture Study: Overview of Architecture and Mission Operations Approach," AIAA SpaceOps 2006 Conference, AIAA Paper 2006-5935, Rome, Italy, June 2006.

[2]May, T. A., " NASA's Space Launch System: A New National Capability" presented at the IEEE Aerospace Conference, Big Sky, MT, March 2012

[3]Proud, R. W., Bendle, J. R., Tedesco, M. B., and Hart, J. J., "Orion Guidance and Control Ascent Abort Algorithm Design and Performance Results," Document Number AAS09_092, Proceedings of the 32nd Annual AAS Guidance and Control Conference, February 2009

[4]McNamara, S. J., Restrepo, C. I., Medina, E. A., Whitley, R. J., Madsen, J. M., and Proud, R. W., "Gain Scheduling for the Orion Launch Abort Vehicle Controller," AIAA Paper 2011-6259, Aug 2011.

[5]P. G. Buning, R. J. Gomez, and W. I. Scallion, "CFD Approaches for Simulation of Wing-Body Stage Separation," AIAA Paper 2004-4838, AIAA 22nd Applied Aerodynamics Conference, Providence, RI, Aug. 2004.

[6]Jespersen, D. C., Pulliam, T. H., and Buning, P. G., "Recent Enhancements to OVERFLOW," AIAA Paper 97-0644, Jan. 1997.

[7]Rogers, S. E., Roth, K., Nash, S. M., Baker, M. D., Slotnick, J. P., Whitlock, M., and Cao, H. V., "Advances in Overset CFD Processes Applied to Subsonic High-Lift Aircraft," AIAA Paper 2000-4216, Aug. 2000.

[8]Chan, W. M., "The Overgrid Interface for Computational Simulations on Overset Grids," AIAA Paper 2002-3188, June 2002.

[9]Rogers, S. E., Suhs, N. E., and Dietz, W. E. "PEGASUS 5: An Automated Pre-processor for Overset-Grid CFD," *AIAA Journal*, Vol. 41, No. 6, June 2003, pp. 1037–1045.

[10]Aftosmis, M. J. and Rogers, S. E., "Effects of Jet-Interaction on Pitch Control of a Launch Abort Vehicle", AIAA Paper 2008-1281, Jan. 2008.

[11]Rogers, S. E. and Pulliam T. H., "Computational Challenges in Simulating Powered Flight of the Orion Launch Abort Vehicle," AIAA Paper 2011-3339, June 2011.

[12]Childs, R. E., Garcia, J. A., Melton, J. E., Rogers, S. E., Shestopolov, A. J., and Vicker, D. J., "OVERFLOW Simulation Guidelines for Orion Launch Abort Vehicle Aerodynamic Analysis," AIAA Paper 2011-3163, June 2011.

[13]Childs, R. E., Garcia, J. A., Rogers, S. E., and Vicker, D. J., "Overflow Aerodynamic Simulation of the Orion Launch Abort Vehicle," presented at the JANNAF 33rd Exhaust Plume and Signatures Meeting, Monterey, CA, Dec., 2012.